Blockade of IL-6 inhibits tumor immune evasion and improves anti–PD-1 immunotherapy

Wenhui Ma (mawenhui891214@163.com)
Nanfang Hospital, Southern Medical University

Wenyi Li
Nanfang Hospital, Southern Medical University

Zhaokun Wu
Nanfang Hospital, Southern Medical University

Chaoting Zhang
Nanfang Hospital, Southern Medical University

Mingzhen Cheng
Nanfang Hospital, Southern Medical University

Yuehong Chen
Nanfang Hospital, Southern Medical University

Yini Zou
Nanfang Hospital, Southern Medical University

Kejun Li
Nanfang Hospital, Southern Medical University

Simin Lin
Nanfang Hospital, Southern Medical University

Wenjun Xiong
Nanfang Hospital, Southern Medical University

Ying Wang
Southern Medical University

Yixiong Lin
Nanfang Hospital, Southern Medical University

Weidong Meng
Nanfang Hospital, Southern Medical University

Weijie Zhou
Nanfang Hospital, Southern Medical University

Research Article

Keywords: Colorectal cancer (CRC), IL-6, tumor immune evasion, CD8+ T cell infiltration, MHC-1 molecules, anti-IL-6, anti-PD1

Posted Date: March 9th, 2022

DOI: https://doi.org/10.21203/rs.3.rs-1420368/v1

Abstract

Background

Long-standing inflammatory bowel disease predisposes to the development of colorectal cancer (CRC). Interleukin (IL) -6, a pivotal link between chronic inflammation and tumor progression, has recently been recognized as a potential target. The effect of IL-6 on proliferation and metastasis of CRC by activating STAT3 pathway has been widely demonstrated in recent years, but few on mediating tumor immune evasion has been reported.

Methods

In this study, we analyzed IL-6 gene expression in human CRC tissues and carried out survival probability in CRC patients with TCGA Data portal and GEO Database. We studied CRC tumorigenesis in vivo by inoculating MC38 tumors and induced-CRC model via AOM/DSS azoxymethan / dextran sulfate sodium in (IL-6 deficient) IL-$6^{-/-}$ and (wild type) WT mice. We measured tumor growth and detected $CD8^{+}$ T cells via immunofluorescence, we validated the function of IL-6 in tumorigenesis and tumor immune evasion in subcutaneous transplantation models. Using endoscopy monitoring and immunofluorescence, we validated the function of IL-6 in tumor immune evasion in AOM/DSS models. We conducted colitis model with DSS reveal the relationship of IL-6 and MHC-1 molecules by qRT-PCR and bioinformatics analysis. Organoid and CRC cells culture, western blot analysis, and qRT-PCR were used to investigate the expression and significance of MHC-1 molecules in vitro without IL-6 stimulation. MHC-1 molecules levels were also detected in tumors of IL-$6^{-/-}$ and WT mice from MC38-bearing tumor models and AOM/DSS models. Subcutaneous MC38 implantation models in C57BL/6 J mice were established to investigate anti-IL-6 therapy on CRC tumorigenesis. In vivo efficacy were conducted using antibodies blocking IL-6 and PD-1 in mice subcutaneous-bearing different types of tumors.

Results

Bio-information analysis and results of our center founded that IL-6 was remarkably overexpressed in CRC and its elevation was associated with poor prognosis. We observed that IL-$6^{-/-}$ mice were less susceptible to develop tumors, compared to (wild type) WT mice. Interestingly, infiltrated $CD8^{+}$ T cells were found to exhibit high expression in tumor of IL-$6^{-/-}$ mice. High level of IL-6 was found in colitis model, with down-regulation of MHC-1molecules. Moreover, in vitro experiments, we found that IL-6 may act as a negative regulator in IFNγ-STAT1-MHC-1 signaling. In addition, vivo trials also confirmed that MHC-1 mRNA levels are negatively related to the existence of IL-6. Furthermore, blockade of IL-6 also activated $CD8^{+}$ T-cell accumulation and led to the high PDL-1 expression in CRC, which can sensitize animals to anti-PD-1 therapy. Importantly, compared to treatment with anti-IL-6 alone and single treatment of anti-PD-1, combined IL-6 and PD-1 blockade greatly improved the therapeutic effect, not only in CRC but also melanoma and breast cancer.

Conclusions

Our study demonstrated that IL-6 act as a negative regulator in immunological surveillance to promote tumor immune evasion by inhibiting the response of cell to IFNγ. Blocking IL-6 enhanced tumor response to anti-PD-1 therapy via infiltration of $CD8^+$ T cell and high expression of PDL-1. Based on the findings of our study, IL-6 is a novel target to improve the efficacy of immunotherapy.

Background

Colorectal carcinoma (CRC) is one of the most common lethal malignancies and the third most prevalent cancer worldwide [1, 2]. Patients with long-standing and poorly controlled inflammatory bowel disease (IBD), such as ulcerative colitis (UC), predispose to CRC than in the general population [3–5]. IBD increases CRC risk and accelerates progression of it. The tumor-promoting effect of chronic inflammation has been generally acknowledged [6]. However, the molecular links between IBD and CRC remain obscure despite their great pathogenic significance [7, 8]. To investigate the location and pathologic appearance of human colitis-associated cancer, have been widely used in the identification of various mechanisms of tumorigenesis [9]. Blocking programmed cell death 1 (PD1) /PD1 ligand 1 (PD-L1) is a strategy to treat a subset of CRC [10–12], such as the microsatellite instability-high (MSI-H) tumors [13, 14]. However, microsatellite stability (MSS) CRC lack of $CD8^+$ T cells infiltration, have been regarded as immune resistance and ineffective to PD-1 /PDL-1 antibodies [15–17]. It is well documented that strong correlations between the number or type of tumor-infiltrating $CD8^+$ T cells and favorable outcomes [18, 19]. In addition, PD-1 /PDL-1 antibodies are breakthroughs for many cancers, including melanoma [20]. However, many cancers like triple negative breast cancers are resistance of the treatment of anti-PD-1/PDL-1 [21]. Thus, developing more available treatments to strengthen the effect of anti-PD-1 /PDL-1 antibodies is extremely urgent, but much less intensive studies have been applied to clinic.

Proinflammatory cytokines play critical roles in almost every stage of tumorigenesis, from initiation and tumor promotion to malignant progression and metastatic spread [5]. IL-6 acts as an indispensable coordinator between chronic inflammation and cancer, where they often plays a crucial role in disease activity and response to therapy [22–24]. High expression of IL-6 are always observed in chronic inflammatory conditions, such as Inflammatory bowel disease [22, 25]. It has been confirmed that high expression of IL-6 in the serum of patients correlated with colon carcinoma and tumor size [26–28]. Elevated levels of IL-6 stimulate hyper activation of STAT3 signaling, which is a major intrinsic pathway for inflammation-related cancer [29, 30]. IL-6/GP130/STAT3 signaling are well known for its role in tumor cell proliferation, survival, and invasion [29, 31].STAT1 and STAT3, competing for the same receptor phosphotyrosine motif, are proteins having similar structure, but they have extremely opposing biological effects on cell growth and survival [32–34]. STAT3 is considered as an oncogene, while activated STAT1 triggers immune surveillance via upregulating the expression of MHC-1 molecules in tumor cells [35–39]. However, it is rarely reported about IL-6 on mediating tumor immune evasion.

Materials And Methods

Patients and samples

This study was approved by the Ethics Committee of Nanfang Hospital (Guangzhou, China). Fresh tissue samples were collected from Department of Pathology, Nanfang Hospital. All patients given informed consents. None of these patients received chemotherapy or radiotherapy before operation.

Cell culture

Murine CRC cell lines (MC38, CT26), murine melanoma cell lines (B16F10) and murine breast cancer cell line (4T1) were kindly gifted by W. Yang of Southern Medical University. All cell lines were cultured in DMEM medium with 10% fetal bovine serum (Gibco), containing at 37 °C, in the atmosphere of 5% CO_2. In addition, mycoplasma contamination was detected via PCR technique.

Crypt isolation and organoid culture

Mouse intestinal crypts were dissociated and cultured according to the protocols of Hans Clever [40]. We made a few modifications in isolation. Isolated small intestines from C57BL/6 mice were opened longitudinally, and rinsed with cold phosphate-buffered saline (PBS) until without any visible debris. The tissue was cut into 5 mm pieces and was collected in a 50 ml conical centrifuge tube containing 30 mL shaking buffer (1 unit/ml of penicillin, 1 μg/ml of streptomycin, and 2.5 ng/ml of amphotericin B in PBS). The tube was swung on a tube rotator (QB-208, Kylin-Bell) at 80 rpm for 10 min (4°C). Discarded supernatant, segments were rinsed with 5 ml cold shaking buffer. Repeated the previous steps. Intestinal segments were changed to 30 ml EDTA chelation buffer (15 mM EDTA in shaking buffer), shaken on a tube rotator for 30 min, and then shocked vigorously for 30 sec on VORTEX-5 (Kylin-Bell). The supernatant with villous debris was discarded; the sediment was resuspended with shaking buffer and 2 min oscillated shakily. Dissociated intestinal crypts were filtered through 70 mm strainers. Collected supernatant were rotated at 200 g for 10 min at 4°C to collect
intestinal crypts. Sedimentation were resuspended in intestinal organoid growth medium, counted, and embedded in Matrigel (growth factor reduced, phenol red free; BD Biosciences) on ice, and planted 50 μl/well in 24-well plates (100 crypts / well) for 30 minutes at 37°C, and overlaid with 500 ul intestinal organoid growth medium. Intestinal organoid growth medium, also called ENR culture medium, it contains DMEM/F12(Invitrogen), 2 mM Glutamax, 10 mM HEPES, 100 U/ml penicillin, 100 μg/mL streptomycin (Invitrogen), 1 mM N-acetyl cysteine (Sigma), B27 supplement (Invitrogen), N2 supplement (Invitrogen), 50 ng/ml mouse EGF (Peprotech), 100 ng/ml mouse Noggin (Peprotech) and 100 ng/mL R-spondin-1 (R&D Systems) or 10% human R-spondin-1-conditioned medium from R-spondin-1-transfected HEK 293T cells).

Hematoxylin eosin & Immunofluorescence staining

The fixed colon tissue was rolled into a so-called “Swiss roll” and dehydrated. A thickness of 2.5 μm Paraffin-embedded sections were obtained and stained with H&E solution. For immunofluorescence staining, frozen colonic tissues and subcutaneous tumors were used to obtain 5 μm sections for subsequent staining. Frozen sections were incubated with anti-CD8 (1:200, #100716, Biolegend) and PDL-1(1:50, #13684S, Cell Signaling Technology). Followed by secondary antibodies and fluorescent reagents goat anti-rat IgG with fluorescein-Cy3 (Perkin Elmer). Nucleus were highlighted using DAPI. Positive expression was evaluated under inverted confocal microscope (LSM880, Olympus).

Total RNA extraction and real-time quantitative PCR

Total RNA of scraped colonic mucosa or cultured organoid/ cells were isolated from Trizol reagent (TaKaRa, Dalian China) following manufacturer's instruction. cDNA synthesis was performed according to the instruction of PrimeScript™ RT reagent Kit (TaKaRa, Dalian China). qRT-PCR was carried out using SYBR *Premix Ex Taq*™ II (TaKaRa, Dalian China) and 7500-fast instrument (Applied BioSystems). Data were normalized to the mean Ct values of housekeeping gene GAPDH and presented as $2^{-\Delta\Delta Ct}$.

Immunoblot analysis

Cultured cells or organoids were lysed with SDS lysis buffer (KeyGEN, Jiangsu, China). Equal amounts of protein extracts were separated by electrophoresis in 10%SDS-PAGE gel and then transferred to PVDF membrane (Merck Millipore, MA, US). After 5% fully Skimmed milk blocking, the PVDF membrane were incubated with the primary antibody anti-GAPDH (1:1000, #60004-1-Ig, Proteintech), anti-Phospho-STAT3(1:300, #9145S, Cell Signaling Technology), anti-STAT3 (1:100, #124H6, Cell Signaling Technology), anti-Phospho-STAT1 (1:100, #9167S, Cell Signaling Technology), anti-STAT1 (1:500, #9172S, Cell Signaling Technology) and anti-IRF1 (1:500, #8478S, Cell Signaling Technology). Signals were detected using horseradish peroxidase (HRP)-conjugated secondary antibodies and Super Signal West Femto Chemiluminescent Substrate (34096, Thermo Fisher Scientific). Images were captured and analyzed using the Image Lab Software (Tanon 5200).

Mice

Female and male C57BL/6, BAL b/c (Guangdong Medical Laboratory Animal Center) and IL-$6^{-/-}$ mice (Jackson) were used at 8–12 weeks of age. Mice were housed in pathogen free environments and were allowed for free access to water and food. Animal related research protocols were conformed to the U.S. Public Health Service Policy on Use of Laboratory Animals. All treatments described were approved by the Ethics Committee on Use and Care of Animals of Southern Medical University.

AOM/DSS models

Chemically-induced colorectal cancer model was achieved by a single intraperitoneal injection of 10 mg/kg azoxymethane (AOM, Sigma-Aldrich,) followed by addition of dextran sulfate sodium salt (DSS MP Biomedical, M.W. 36,000-50,000 kDa) to the drinking water at a concentration of 2.5% for 5 days (first DSS cycle). This was followed by 10 days of regular sterile water for recovery, and this DSS cycle was repeated twice. The mice were sacrificed by cervical dislocation on day 100 and the colons were removed.

Colitis models

For colitis induction, mice were supplied with 2% of DSS dissolved in distilled drinking water for 5 days, followed by 5 days of regular drinking water, and sacrificed for colon tissue on day 21. Histopathological analyses and PR-PCR were performed according to standard methods.

Subcutaneous tumor models

MC38 cells (1×10^6) suspended in 200 μl PBS were injected respectively subcutaneously into the right hind limb of 8-12 week male wild type (WT) C57BL/6 mice and IL-$6^{-/-}$ mice (n = 6 each group).

MC38 cells (1×10^6), CT26 cells (1×10^6), B16F10 (5×10^5) cell and 4T1 (1×10^6) were resuspended in 200 μl PBS and implanted subcutaneously into the flank of 8-12 week male C57BL/6 mice for MC38 and B16F10 and BALB/c for CT26 and 4T1 (n = 8 each group).

Tumor size was measured every day with a Vernier caliper, and tumor volume was counted as $0.5\times L\times W^2$ (cm^3; L stands for length and W for the width of the tumor).

Mice were killed at indicated days after injection. Tumors were detached, measured and recorded. Each tumor divided into two part. One part was made into frozen section for further immunofluorescence assessment and other was fixed with formalin and embedded in paraffin for HE.

Treatment of mice with anti-IL-6 and anti-PD-1

Treatment with IL-6 antibodies (#BE0046, BioXcell) or/and PD-1 antibodies (#BE0146, BioXcell) was started when the tumor volume in mice reached 100 mm^3, while the control group injected isotype (BE0089, BioXcell). The treatments were administered by intraperitoneal injection, 100 μg per mouse every three day until sacrifice.

Endoscopic observation

Mice were anesthetized by inhaling 1.5 % isoflurane (RWD Life Science Co, Ltd, Shenzhen, China). Optical colonoscopy was performed using a Karl Storz (Tuttlingen, Germany) Image 1 HD Camera System. After AOM/DSS induction or DSS-induced model, colitis or tumor were monitor and scored by endoscopy as described previously.

Statistical analysis

Data were all summarized with mean ± standard error of mean (SEM) unless stated otherwise. The unpaired two-tail student's t-test was used for experiments where two means were compared, unless indicated. For three or more groups with two parameters, one-way or two-way analysis of variance (ANOVA) was used. Datasets used for IL-6 expression paired comparison and survival analysis in R (version 4.0.3) were downloaded from The Cancer Genome Atlas (TCGA) and Gene Expression Omnibus (GSE20916, GSE17538, and GSE41258). Survival analysis was performed using "survminer" package. In brief, "surv_cutpoint" function to find optimal cutpoint and log-rank P value based on IL-6 expression, and "survfit" function was used to fit overall survival time and status. Statistical analyses were performed using GraphPad Prism software 5.0 (CA, US) and SPSS software (Version 22.0, IL, US).

Results

Up-regulated IL-6 expression is tightly associated with worse prognosis of CRC.

To understanding the role of IL-6 in CRC, we analyzed the expression of IL-6 in GEO database (GSE20916) and in TCGA paired-CRC tissues. High level of IL-6 was detected in cancer tissues compared with normal tissues (Fig. 1A & B). Data from our center confirmed that IL-6 was remarkably overexpressed in CRC. Furthermore, higher IL-6 expression was significantly associated with a shorter overall survival (OS) of CRC patients in our center (Fig. 1D). In addition, using GSE17538 dataset, optimal survival cut-off was found based on Log-Rank *p* value (Fig. 1E & F), and higher IL-6 indicated unfavorable prognosis in CRC patients (Fig. 1G). Similar results were obtained in GSE41258 data set (Fig. H-J). Overall, these results implied that IL-6 might act as a pro-tumor factor of CRC and high expression was indeed associated with worse prognosis.

Deficiency of IL-6 in the mice suppresses tumorigenesis and improves accumulation of $CD8^+$ T cells in vivo

To examine the significance of IL-6 in tumorigenesis, we used a previously established murine colon carcinoma model based on the mutagenic agent azoxymethan (AOM) and dextran sulfate sodium (DSS) on IL-$6^{-/-}$ mice or WT littermates. Colon tumorigenesis was chemically induced by a single injection of azoxymethane (AOM) followed by three 7-day cycles of dextran sodium sulfate (DSS) to create a chronic inflammatory state (Fig. 2A). Next, we monitored tumor development longitudinally by small animal colonoscopy. After 86-day AOM/DSS treatment, less and smaller tumors in the colons of IL-$6^{-/-}$ mice were observed, compared to WT mice (Fig. 2B). By gross observed, IL-$6^{-/-}$ mice had less tumors distributed from the distal end of the medial part of the colon (Fig. 2C). Tumors occurred more infrequently and tumor loads were more minor in IL-$6^{-/-}$ mice than in WT mice (Fig. 2D&E). We then conducted immunofluorescent analyses to detect $CD8^+$ T cells infiltrating in colon malignant tissues (Fig. 2F). Interestingly, the number of Infiltrated $CD8^+$ T cells in tumors were higher in tumor tissues of IL-$6^{-/-}$ mice than in those of WT mice (Fig. 2G). To further confirm the lack of IL-6 in the mice suppresses tumorigenesis, murine MC38 colorectal cancer cells were intradermal injected into WT and IL-$6^{-/-}$ mice. Tumor size and weight were notably reduced in IL-$6^{-/-}$ mice compared with WT mice (Fig. 2H-J). We further investigated the $CD8^+$ T cells infiltrating into tumor tissues in WT and IL-$6^{-/-}$ mice. As a result, $CD8^+$ T cells were accumulated in tumor environments of IL-$6^{-/-}$ mice compared with WT mice (Fig. 2K & L). These data provide evidence that bare of IL-6 protects against tumorigenesis and facilitate introduction of $CD8^+$ T cells infiltrating into the tumor.

IL-6 produced in vivo suppress the expression of MHC-1 molecules

Using GSE9281 dataset, we observed that the expression of IL-6 first increased and then decreased in colitis rats (Fig. 3A). MHC-1 molecules of rats, such as RT1-A2 and RT1-S3 showed the opposite trend (Fig. 3B & C). To further explore the potential role of between IL-6 and MHC-1, WT mice were orally treated with 5-day 2%DSS (Fig. 3D). After induction of colitis, colitis severity was scored and monitored on day 0, 1,5,9,11,21 by small animal colonoscopy. We found that, the severity of colitis was greatest on day 7-9 and then shown gradual improvement (Fig. 3E & F). In addition, the bowels were resected from DSS-treated WT mice on different days and subjected to macroscopic and histopathological inflammation score. The severity of colitis was greatest on day 7 and then recovered gradually (Fig. 3G). The gross appearance of the organs from DSS-treated WT mice showed apparent shortening of the colon tissue, especially day 7 (Fig. 3H & I). Consistent with these findings are the results obtained by HE staining, which demonstrated that the WT animals drinking DSS water showed obvious manifestations of inflammatory colitis, especially day 7-9, including crypt epithelial cell apoptosis, mucosal erosions, ulcers, and inflammatory cell infiltration (Fig. 3J). The colonic mucosa was collected from DSS-fed mice every other day until day21 for QPCR. In the occurrence of colitis, IL-6 was first increased until day 7 and then decreased in the WT colon (Fig. 3K). Interestingly, the

expression of MHC-1 molecules H2-D1 and H2-K1 showed a totally different variation trend (Fig. 3L & 3M). Together, these data confirm a negative relationship between IL-6 and MHC-1 molecules.

IL-6 deficiency induced the high expression of MHC-1 in vitro and in vivo

It is well documented that STAT3 can antagonize STAT1 in apoptosis , angiogenic, and metastatic of tumor[32, 33]. Using interferon-gamma (IFNγ) stimulate, more STAT1 phosphorylation increases the activation of $CD8^+$ T cell-mediated anti-tumor responses [34, 38]. To this end, we further explored the possibility that IL-6 effects the expression of MHC-1 molecules via JAK/STAT3 signaling pathway.

We derived small intestinal crypt from WT mice and added IFNγ and IL-6 together or respectively with different concentration (Fig. 4A). Next, we examined the changes of signaling by western blotting. With the existence of IL-6, the level of STAT3 phosphorylation increased, while IFNγ induced STAT1 phosphorylation and IRF1 upregulation was inhibited significantly (Fig. 4B). IL-6 also remarkably decreased the mRNA expression of MHC-1 molecules induced by IFNγ in small intestinal crypt-derived organoids, including H2-D1 and H2-K1 (Fig. 4C). Furthermore, CT26 cells were also cultured and examined the changes of these signaling. The similar results were observed in the CT26 cell model. Adding IL-6, STAT3 phosphorylation was upregulated and the IFNγ-STAT1 pathway was downregulated by immunoblot analysis (Fig. 4D). Meanwhile, the addition of IL-6 decreased the IFNγ-induced MHC-1 molecules mRNA levels in CT26 cells (Fig. 4E).

From the DSS model, histological analysis exhibited severe colitis in WT and IL-6 mice. Random and disorganized gland , crypt loss, goblet cells increased and more extensive inflammatory cell infiltration reaching the submucosa in the colon of day 7 ,compared with day 0 in WT mice, while $IL\text{-}6^{-/-}$ displayed severe inflammation with focal areas of ulceration, necrotic lesions, accumulation of palisading granuloma and infiltration of lymphocytes (Fig. 4F). Upon DSS treatment, we collected colonic mucosa of WT and IL-6 mice from day 0 and day 7, and performed a Q-PCR assay to assess mRNA expression of H2-K1 and H2-D1. Under inflammatory condition, expression of H2-K1 and H2-D1 was preferentially enriched in $IL\text{-}6^{-/-}$ mice, compared to WT mice (Fig. 4G & H). We then analyzed the intratumoral expression of H2-K1 and H2-D1 from the AOM/DSS model and MC38 tumor-bearing WT and IL-6 mice. Strikingly, in tumor environments, mRNA expression of H2-K1 and H2-D1greater accumulated in $IL\text{-}6^{-/-}$ mice (Fig. 4I &J). Collectively, these results indicate that deficiency of IL-6 would restrain STAT3 signaling pathway to elevate the expression of MHC-1.

IL-6-neutralizing antibodies provide anti-tumor efficacy with significant infiltration of $CD8^+$ T cells via increasing the expression of MHC-1 and PD-L1

To validate the contribution of anti-IL-6 in immune response to tumor, CT26 tumor-bearing WT mice were then administered anti-IL-6 or isotype as a control. Striking, we observed a significant decrease in tumor size, growth, and weigh after anti-IL-6 treatment compared with isotype control (Fig. 5A-C).

Next, we observed $CD8^+$ T cells infiltrating in the endpoint subcutaneous tumors from two groups via immunofluorescent analyses (Fig. 5D). The immunofluorescent results confirmed that IL-6-neutralizing antibodies increased $CD8^+$ T cells in the CT26 subcutaneous tumor sections (Fig. 5E). Importantly, the mRNA expression of H2-K1 and H2-D1 were robustly upregulation in the tumor of IL 6-neutralizing antibodies-treating mice (Fig. 5F & G).

Surprisingly, blocking IL-6 dramatically upregulated the PD-L1 mRNA expression in subcutaneous CT26 tumors (Fig. 5H). In addition, the immunofluorescent results also suggested that the expression levels of PD-L1 were directly augmented with administered anti-IL-6 (Fig. 5I & J). Together, these results reveal that blocking IL-6 mediates anti-tumor efficacy of $CD8^+$ T cells by enhancing the levels of MHC-1 and PD-L1 in tumors.

Blocking IL-6 enhances tumor response to anti-PD-1 immunotherapy

It is well reported that CT26 cell line represents an MMR-proficient colorectal cancer type [41] and 4T1 is poorly immunogenic cancer [42]. This two cell lines is well proven to be resistant to anti-PD1 treatment [43].To evaluate the capacity of anti-IL 6 antibodies to enhance the sensitivity of anti-PD1 antibodies, the efficacy of co-administration of anti-IL-6 and anti-PD-1 on different subcutaneous tumor models, such as MC38, CT26, 4T1 and B16F10, were examined (Fig. 6A). We found that blocking IL-6 or PD-1 alone resulted in some therapeutic effect on MC38 and B16F10 subcutaneous tumors compare to isotype control group. Strikingly, combined treatment further inhibited tumor growth compare to isotype control group and other single treatments (Fig. 6E-J).

Next, we demonstrated whether anti-IL-6 could synergize with immune checkpoint blockade therapy. As expected, single treatment with anti-PD-1 or anti-IL-6 had a partial effect on CT26 tumor volume and tumor weight. When combining anti-PD-1 with anti-IL-6, such improvement was exhibited a notable delay in the tumor growth, decrease in the tumor weight of CT26 tumor-bearing mice (Fig. 6B-D). In addition, the 4T1 tumor-bearing model showed a similar result that, compared with that single treatment, 4T1 tumor size, growth and weight were significantly diminished by the combined treatment (Fig. 6K-M). These results indicate that anti-IL-6 and anti-PD-1 treatment suppress tumor growth significantly. Therefore, the combination of anti-IL-6 and anti-PD-1 is a prospective way to CRCs therapy.

Discussion

IL-6 represents a minor subset of cytokines in inflammation-associated tumorigenesis. Accumulating evidence suggests its role in the orchestration of proliferation and metastasis in tumor [44]. In the present study, IL-6 is a significant cytokine in inflammation-associated tumorigenesis selected from database and our medical center biobank, which is upregulated, and related to tumorigenesis and poor prognosis of CRCs.

Many researches have validated that the enrichment of $CD8^+$ T cells indicates a favorable prognosis for patients with CRC [18]. In poor prognosis of CRCs, tumor cells have been reported escape from the attack of $CD8^+$ T cell by abolishing MHC-1 antigen presentation [45]. This research was intended to further explore the function of IL-6 in tumor evasion. In AOM/DSS models, increased $CD8^+$ T cell infiltration was responsible for the decrease of tumors in IL-$6^{-/-}$ mice, compared to WT mice; however, similar result was found in subcutaneous models. Later, we did an analysis of the database and in vivo experiment, a negative correlation was found between IL-6 and MHC-1 molecules. Vitro investigations revealed that IL-6 primarily activates STAT3 phosphorylation. Since the phosphorylation of STAT1 and STAT3 is usually in an equilibrium state, we reasonably arrived at the conclusion that IL-6 downregulated JAK/STAT1 signaling indirectly, resulting in the suppression of expression of MHC-1 genes. IFNγ up-regulates MHC-1 antigen presentations via activation of JAK/STAT1 signal transduction pathway, of which tumors might be susceptible to immunological surveillance [39]. Herein, we observed that IL-6 upregulated the expression of phosphorylated STAT3, which had the negative effect on the STAT1 phosphorylation, revealing that MHC-1 molecules are indirectly downregulated by IL-6 in the CRCs.

Monoclonal antibodies against IL-6 have been developed for clinical application, such as siltuximab [46]. As a single drug, Siltuximab has minimal effect on tumor inhibition, but exerts significant effect when combining with other antitumor treatments [47]. Due to immunological resistance mechanisms in CRC, IL-6 monotherapy is not an effective strategy to kill tumor cells.

Our results have confirmed that blocking IL-6 is sufficient to activate IFNγ-STAT1 signaling and increase $CD8^+$ T cell infiltration via hyperactivation of MHC-1 and PDL-1 expression in CT26 tumors. Thus, the use of IL-6-blocking antibodies is a novel strategy for enhancing the sensitivity of tumors to anti-PD-1 treatment (Figure 6N).

Anti-PD-1/PDL-1 are widely applied to treat tumors carrying sensitive immune checkpoint inhibitor [10]. However, anti-PD-1/PDL-1 therapy is ineffective to tumors associated immune evasion and resistance to immune checkpoint inhibitor [15]. Recently, more and more investigations have revealed that anti-IL-6 co-administered with anti-PD-1 displays a significant role in antitumor [48, 49]. However, the mechanism underling the combination treatment is not completely clear.

Hence, anti-IL-6 repositioning emerges as a new approach to treat MSS-CRC and immune-resistance tumors. Our finding has observed that the absence of IL-6 abolished the tumor immune evasion and promoted infiltrated $CD8^+$ T cell, suggesting that IL-6 plays an indispensable role in evading immunological surveillance. Blocking IL-6, tumor exhibited higher MHC-1 and PDL-1 to up-regulate

immune checkpoint inhibitor, which can enhance tumor responses to anti-PD-1. However, the potential mechanism of IL-6 in tumor escape is still unclear. Furthermore, we therefore decided to dig deeper and reveal the mechanism more in detail.

Conclusions

This study presented that IL-6 is significantly upregulated in CRC via bio-information analysis. Deficiency of IL-6 promoted $CD8^+$ T cells infiltrating tumors via upregulating the expression of MHC-1 molecules and PDL-1, which could sensitize CRC to anti-PD-1 therapy. This research suggests IL-6 as a novel therapeutic target in the CRC.

Abbreviations

CRC, colorectal cancer; IBD, inflammatory bowel disease; UC, ulcerative colitis; PD-1/PDL-1, programmed cell death 1/PD-1 ligand 1; MSI-H, microsatellite instability-high; MSS, microsatellite stability; IL-6, Interleukin -6; AOM/DSS ,azoxymethan / dextran sulfate sodium ; WT, wild type; IL-$6^{-/-}$ mice, IL-6 knock-out mice; PMSF, phenylmethylsulfonyl fluoride; PBS, phosphate Buffered Saline; SDS-PAGE, sodium dodecyl sulfatepolyacrylamide gel electrophoresis; PVDF, Poly (vinylidene fluoride);HRP, Horseradish Peroxidase; qRT-PCR, Quantitative Real-time PCR; GSEA, gene set enrichment analysis; GEO, gene expression omnibus; MHC-1, major histocompatibility complex-1; JAK, janus kinase; STAT, signal transducer and activator of transcription; IFNγ, interferon-g; anti-IL-6, IL-6 antibody; anti-PD-1, PD-1 antibody

Declarations

Ethics approval and consent to participate

All the patients were informed of information collection and usage. The information was collected and analysis in accordance with approval by the Institutional Ethical Committee Board (Nanfang Hospital, Guangzhou, China). Use of animal was approved by the Southern Medical University animal ethic committee.

Consent for publication

Not applicable.

Availability of data and materials

The datasets generated during and/or analyzed during the current study (GSE20916, GSE17538, GSE41258 and GSE9281) are available in Gene Expression Omnibus (GEO) database,

“https://www.ncbi.nlm.nih.gov/geo/query/acc.cgi?acc=GSE20916”,
“https://www.ncbi.nlm.nih.gov/geo/query/acc.cgi?acc=GSE17538”,

“https://www.ncbi.nlm.nih.gov/geo/query/acc.cgi?acc=GSE41258” and
“https://www.ncbi.nlm.nih.gov/geo/query/acc.cgi?acc=GSE9281”.

Competing interests

All authors declared no conflict of interests.

Funding

This work was supported by the National Natural Science Foundation of China (81902970), Natural Science Foundation of Guangdong Province (No. 2017A030310115 and No. 2019A1515011325), China Postdoctoral Science Foundation (2019M650205), State's Key Project of Research and Development Plan (2017YFC0108300), Guangdong Provincial Natural Science Foundation for Distinguished Young Scientists (2015A030306048), Guangzhou science and technology collaborative innovation major projects (201704020071).

Authors' contributions

The study was conceived, designed, supervised and drafted the manuscript by YL, WM, WM and WZ. WL, MC, ZW, CZ designed the project, analyzed and interpreted the data. WL, CZ developed mouse models and organoid-related experiments. ZW, YZ carried out western blot analysis. WX, MC, YC performed the bioinformatics, statistical analysis. SL, YZ performed IHC staining and functional experiments. YW, KL, WX, YC collected clinical samples and data for this study. All authors read and approved the final manuscript.

Acknowledgements

We would like to express gratitude to Prof. Guoxin Li and Department of General Surgery, Nanfang Hospital for providing CRC specimens, also towards Central Laboratory of Southern Medical University and its staffs for technical support. Thanks to Lijing Wang and Vascular Biology Research Institute, School of Life Sciences, Guangdong Pharmaceutical University for generously providing breeding pairs of the IL-6$^{-/-}$ mice. Thanks to Side Liu and Department of Clinical Medicine, Nanfang Hospital, Southern Medical University for providing qRT-PCR instrument for use. Additional thanks to all members of the Zhou Laboratory for technical assistance and encouragement.

Competing interest

All authors declared no conflict of interests

References

1. Center MM, Jemal A, Smith RA, Ward E. Worldwide variations in colorectal cancer. CA: a cancer journal for clinicians. 2009;59(6):366-78.
2. Biller LH, Schrag D. Diagnosis and treatment of metastatic colorectal cancer: a review. JAMA. 2021;325(7):669-85.
3. Schäfer M, Werner S. Cancer as an overhealing wound: an old hypothesis revisited. Nature reviews Molecular cell biology. 2008;9(8):628-38.
4. Schmitt M, Greten FR. The inflammatory pathogenesis of colorectal cancer. Nature Reviews Immunology. 2021:1-15.
5. Hoare A, Soto C, Rojas-Celis V, Bravo D. Chronic Inflammation as a Link between Periodontitis and Carcinogenesis. 2019;2019:1029857.
6. Arhi C, Askari A, Nachiappan S, Bottle A, Arebi N, Athanasiou T, et al. Stage at diagnosis and survival of colorectal cancer with or without underlying inflammatory bowel disease: a population-based study. Journal of Crohn's and Colitis. 2021;15(3):375-82.
7. Karin M, Lawrence T, Nizet V. Innate immunity gone awry: linking microbial infections to chronic inflammation and cancer. Cell. 2006;124(4):823-35.
8. Saleh M, Trinchieri G. Innate immune mechanisms of colitis and colitis-associated colorectal cancer. Nature Reviews Immunology. 2011;11(1):9-20.
9. Neufert C, Becker C, Neurath MF. An inducible mouse model of colon carcinogenesis for the analysis of sporadic and inflammation-driven tumor progression. Nature protocols. 2007;2(8):1998.
10. Balar AV, Weber JS. PD-1 and PD-L1 antibodies in cancer: current status and future directions. Cancer immunology, immunotherapy : CII. 2017;66(5):551-64.
11. Gong J, Chehrazi-Raffle A, Reddi S, Salgia R. Development of PD-1 and PD-L1 inhibitors as a form of cancer immunotherapy: a comprehensive review of registration trials and future considerations. 2018;6(1):8.
12. Iwai Y, Ishida M, Tanaka Y, Okazaki T, Honjo T, Minato N. Involvement of PD-L1 on tumor cells in the escape from host immune system and tumor immunotherapy by PD-L1 blockade. Proceedings of the National Academy of Sciences of the United States of America. 2002;99(19):12293-7.
13. Overman MJ, Kopetz S, McDermott RS, Leach J, Lonardi S, Lenz H-J, et al. Nivolumab ± ipilimumab in treatment (tx) of patients (pts) with metastatic colorectal cancer (mCRC) with and without high microsatellite instability (MSI-H): CheckMate-142 interim results. Journal of Clinical Oncology. 2016;34(15_suppl):3501-01.

14. Overman MJ, McDermott R, Leach JL, Lonardi S, Lenz HJ, Morse MA, et al. Nivolumab in patients with metastatic DNA mismatch repair-deficient or microsatellite instability-high colorectal cancer (CheckMate 142): an open-label, multicentre, phase 2 study. The Lancet Oncology. 2017;18(9):1182-91.
15. Tumeh PC, Harview CL, Yearley JH, Shintaku IP, Taylor EJ, Robert L, et al. PD-1 blockade induces responses by inhibiting adaptive immune resistance. Nature. 2014;515(7528):568-71.
16. Chalabi M, Fanchi LF, Dijkstra KK, Van den Berg JG, Aalbers AG, Sikorska K, et al. Neoadjuvant immunotherapy leads to pathological responses in MMR-proficient and MMR-deficient early-stage colon cancers. Nature Medicine. 2020;26(4):566-76.
17. Sun R, Limkin EJ, Vakalopoulou M, Dercle L, Champiat S, Han SR, et al. A radiomics approach to assess tumour-infiltrating CD8 cells and response to anti-PD-1 or anti-PD-L1 immunotherapy: an imaging biomarker, retrospective multicohort study. The Lancet Oncology. 2018;19(9):1180-91.
18. Funada Y, Noguchi T, Kikuchi R, Takeno S, Uchida Y, Gabbert HE. Prognostic significance of CD8+ T cell and macrophage peritumoral infiltration in colorectal cancer. Oncology reports. 2003;10(2):309-13.
19. Koch M, Beckhove P, op den Winkel J, Autenrieth D, Wagner P, Nummer D, et al. Tumor Infiltrating T Lymphocytes in Colorectal Cancer: Tumor-Selective Activation and Cytotoxic Activity In Situ. Annals of Surgery. 2006;244(6):986-93.
20. Peggs KS, Quezada SA. PD-1 blockade: promoting endogenous anti-tumor immunity. Expert review of anticancer therapy. 2012;12(10):1279-82.
21. Marmé F, Schneeweiss A. Targeted Therapies in Triple-Negative Breast Cancer. Breast care (Basel, Switzerland). 2015;10(3):159-66.
22. Kumari N, Dwarakanath B, Das A, Bhatt AN. Role of interleukin-6 in cancer progression and therapeutic resistance. Tumor Biology. 2016;37(9):11553-72.
23. Naka T, Nishimoto N, Kishimoto T. The paradigm of IL-6: from basic science to medicine. Arthritis Research & Therapy. 2002;4(3):1-10.
24. McElvaney OJ, Curley GF, Rose-John S, McElvaney NG. Interleukin-6: obstacles to targeting a complex cytokine in critical illness. The Lancet Respiratory Medicine. 2021.
25. Rincon M. Interleukin-6: from an inflammatory marker to a target for inflammatory diseases. Trends in immunology. 2012;33(11):571-77.
26. Scheller J, Chalaris A, Schmidt-Arras D, Rose-John S. The pro-and anti-inflammatory properties of the cytokine interleukin-6. Biochimica et Biophysica Acta (BBA)-Molecular Cell Research. 2011;1813(5):878-88.
27. Chung YC, Chang YF. Serum interleukin-6 levels reflect the disease status of colorectal cancer. Journal of surgical oncology. 2003;83(4):222-26.
28. Groblewska M, Mroczko B, Wereszczyńska-Siemiątkowska U, Kędra B, Łukaszewicz M, Baniukiewicz A, et al. Serum interleukin 6 (IL-6) and C-reactive protein (CRP) levels in colorectal adenoma and cancer patients. Clinical Chemistry and Laboratory Medicine. 2008;46(10):1423-28.

29. Grivennikov S, Karin E, Terzic J, Mucida D, Yu G-Y, Vallabhapurapu S, et al. IL-6 and Stat3 are required for survival of intestinal epithelial cells and development of colitis-associated cancer. Cancer cell. 2009;15(2):103-13.
30. Zhong Z, Wen Z, Darnell JE. Stat3: a STAT family member activated by tyrosine phosphorylation in response to epidermal growth factor and interleukin-6. Science. 1994;264(5155):95-98.
31. Schindler C, Darnell Jr J. Transcriptional responses to polypeptide ligands: the JAK-STAT pathway. Annual review of biochemistry. 1995;64(1):621-52.
32. Avalle L, Pensa S, Regis G, Novelli F, Poli V. STAT1 and STAT3 in tumorigenesis: A matter of balance. Jak-stat. 2012;1(2):65-72.
33. Sara P, Gabriella R, Daniela B, Francesco N, Valeria P. STAT1 and STAT3 in tumorigenesis: two sides of the same coin. Madame Curie Bioscience Database. 2000.
34. Qing Y, Stark GR. Alternative activation of STAT1 and STAT3 in response to interferon-γ. Journal of Biological Chemistry. 2004;279(40):41679-85.
35. Kusaba T, Nakayama T, Yamazumi K, Yakata Y, Yoshizaki A, Inoue K, et al. Activation of STAT3 is a marker of poor prognosis in human colorectal cancer. Oncology reports. 2006;15(6):1445-51.
36. Shen Y, Devgan G, Darnell JE, Bromberg JF. Constitutively activated Stat3 protects fibroblasts from serum withdrawal and UV-induced apoptosis and antagonizes the proapoptotic effects of activated Stat1. Proceedings of the National Academy of Sciences. 2001;98(4):1543-48.
37. Chen Y, Wang J, Wang X, Liu X, Li H, Lv Q, et al. STAT3, a poor survival predicator, is associated with lymph node metastasis from breast cancer. Journal of breast cancer. 2013;16(1):40.
38. Leibowitz MS, Andrade Filho PA, Ferrone S, Ferris RL. Deficiency of activated STAT1 in head and neck cancer cells mediates TAP1-dependent escape from cytotoxic T lymphocytes. Cancer immunology, immunotherapy. 2011;60(4):525-35.
39. Simpson JA, Al-Attar A, Watson NF, Scholefield JH, Ilyas M, Durrant LG. Intratumoral T cell infiltration, MHC class I and STAT1 as biomarkers of good prognosis in colorectal cancer. Gut. 2010;59(7):926-33.
40. Koo B-K, Stange DE, Sato T, Karthaus W, Farin HF, Huch M, et al. Controlled gene expression in primary Lgr5 organoid cultures. Nature Methods. 2012;9(1):81-83.
41. Castle JC, Loewer M, Boegel S, de Graaf J, Bender C, Tadmor AD, et al. Immunomic, genomic and transcriptomic characterization of CT26 colorectal carcinoma. BMC Genomics. 2014;15(1):190.
42. Pulaski BA, Ostrand-Rosenberg S. Reduction of established spontaneous mammary carcinoma metastases following immunotherapy with major histocompatibility complex class II and B7.1 cell-based tumor vaccines. Cancer Res. 1998;58(7):1486-93.
43. Kim K, Skora AD, Li Z, Liu Q, Tam AJ, Blosser RL, et al. Eradication of metastatic mouse cancers resistant to immune checkpoint blockade by suppression of myeloid-derived cells. Proceedings of the National Academy of Sciences of the United States of America. 2014;111(32):11774-9.

44. Uciechowski P, Dempke WC. Interleukin-6: a masterplayer in the cytokine network. Oncology. 2020;98(3):131-37.
45. Doorduijn EM, Sluijter M, Querido BJ, Oliveira CC, Achour A, Ossendorp F, et al. TAP-independent self-peptides enhance T cell recognition of immune-escaped tumors. The Journal of clinical investigation. 2016;126(2):784-94.
46. Weber R, Groth C, Lasser S, Arkhypov I, Petrova V, Altevogt P, et al. IL-6 as a major regulator of MDSC activity and possible target for cancer immunotherapy. Cellular Immunology. 2021;359:104254.
47. Song L, Smith MA, Doshi P, Sasser K, Fulp W, Altiok S, et al. Antitumor efficacy of the anti-interleukin-6 (IL-6) antibody siltuximab in mouse xenograft models of lung cancer. Journal of thoracic oncology : official publication of the International Association for the Study of Lung Cancer. 2014;9(7):974-82.
48. Zhao D, Cai L, Lu X, Liang X, Li J. Chromatin Regulator CHD1 Remodels the Immunosuppressive Tumor Microenvironment in PTEN-Deficient Prostate Cancer. 2020;10(9):1374-87.
49. Liu H, Shen J, Lu K. IL-6 and PD-L1 blockade combination inhibits hepatocellular carcinoma cancer development in mouse model. Biochemical and biophysical research communications. 2017;486(2):239-44.

Figures

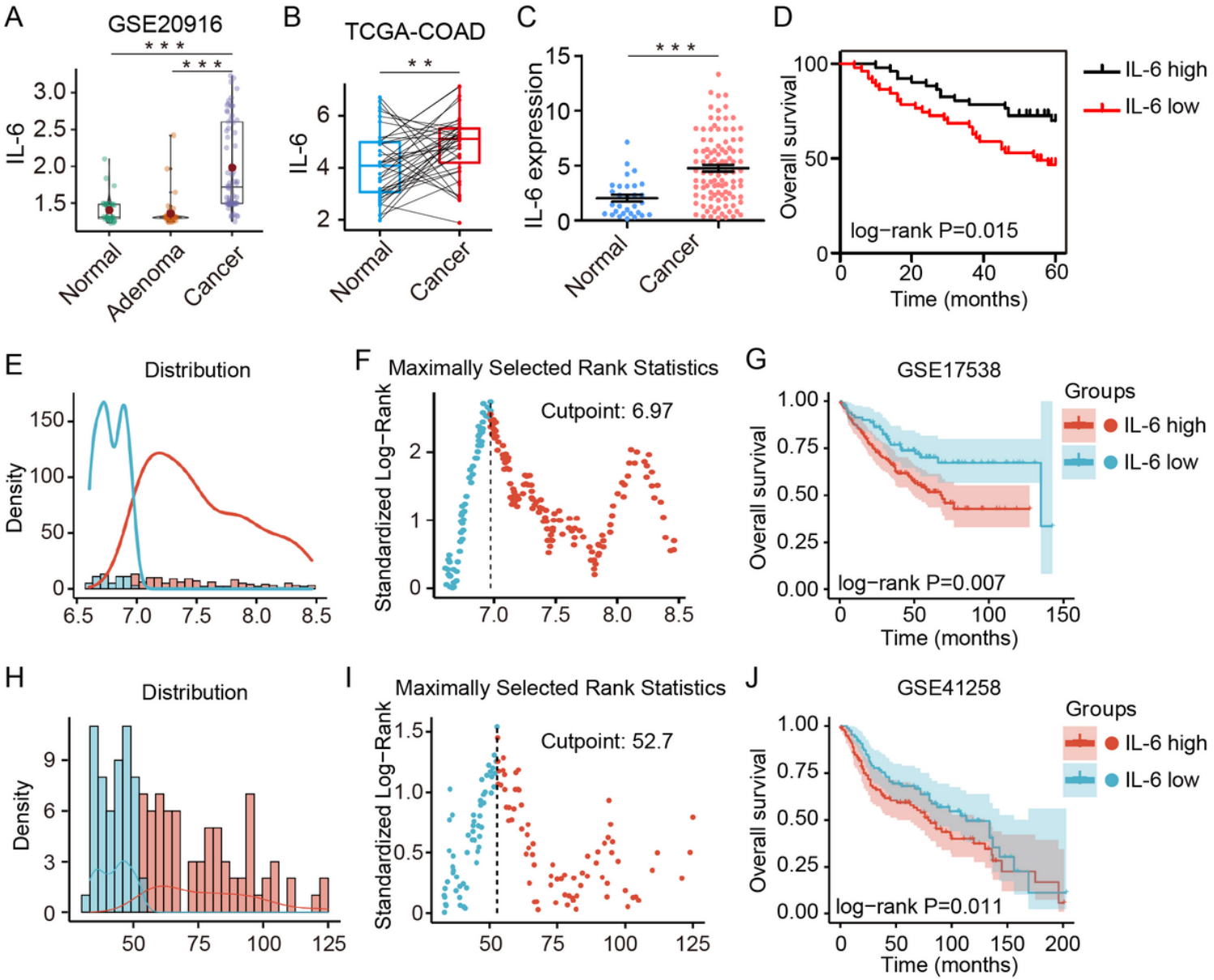

Figure 1

Differential expression of IL-6 indicated unfavorable prognosis in CRC.

A–B IL-6 expression in different tissues from GEO and TCGA datasets. (A) GSE20916 dataset, CRC, normal colon vs. adenoma vs. cancer (*n* =34 *vs.* 54 *vs.* 66). Data were presented as means ± SEM, *** P < 0.001, *t* test. (B-C) TCGA-COAD dataset, paired normal colon *vs.* cancer (*n* =39), means ± SEM, ** P < 0.01, paired-*t* test. **D**. Kaplan-Meier curves of CRC patients' overall survival with high or low IL-6 expression level of internal cohort. Log−Rank P=0.015.**E-J** CRC overall survival analysis based on IL-6 expression. (E-G) GSE17538 (*n* =232), optimal cutpoint = 6.97, log−rank P=0.007. (H-J) GSE41258 (*n* =185), optimal cutpoint = 52.7, log−rank P=0.011.

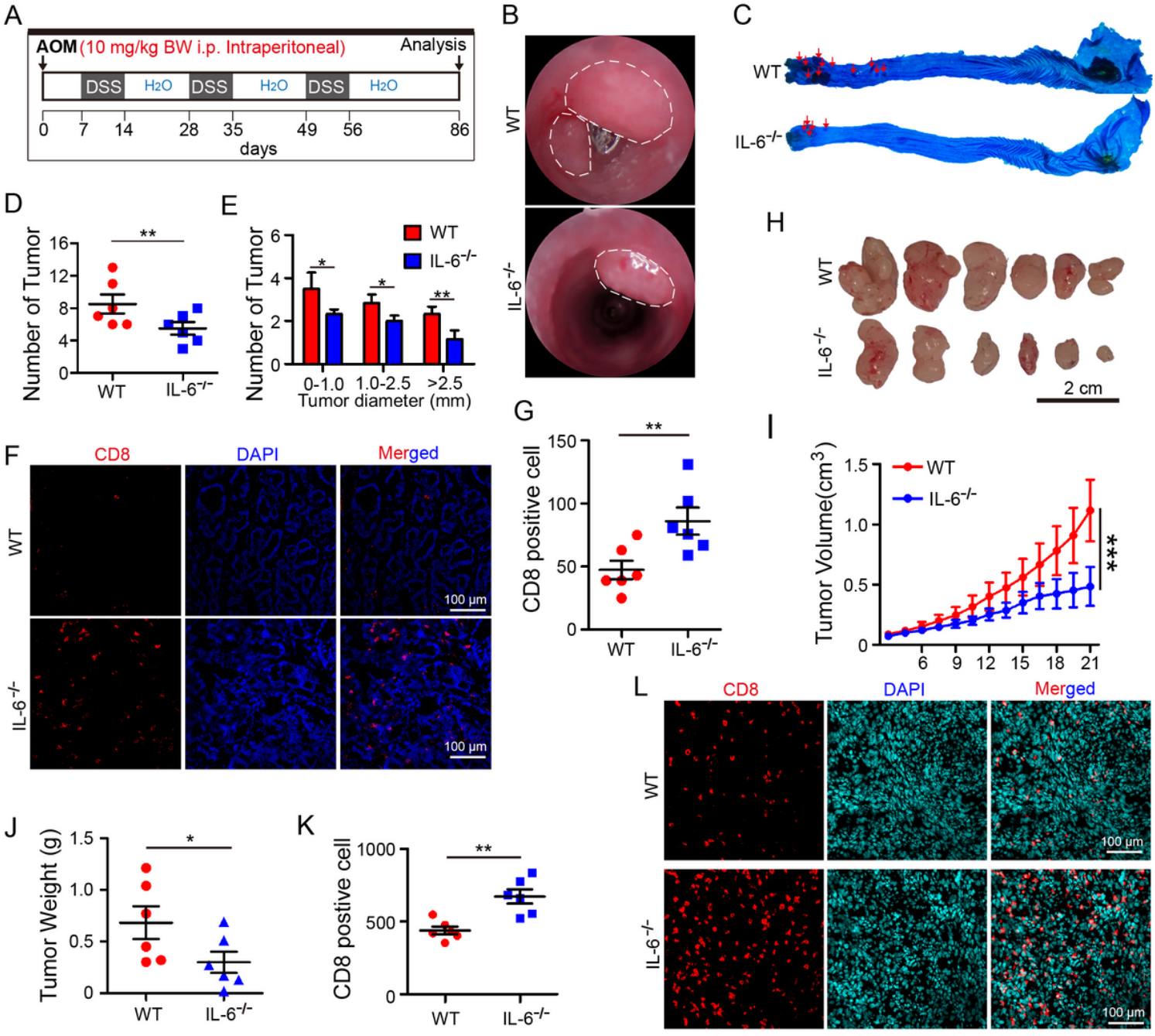

Figure 2

IL-6$^{-/-}$ developed less tumor via improving accumulation of CD8^{+} T cells compared to WT mice

A WT C57BL/6 mice and IL-6$^{-/-}$ mice (n = 6, each group) were at least 8 weeks old before use and throughout the experiments. WT and IL-6$^{-/-}$ mice were given three cycles of DSS (20 mg/mL) after intraperitoneal treatment of AOM (10mg/kg). After induction of tumorigenesis (86 days), mice were euthanized and colons were collected. **B** Representative optical colonoscopy of tumors formed after AOM/DSS treatment into WT C57BL/6 and IL-6$^{-/-}$ mice and the tumor formation were shown. **C** Representative images of colon tumors with a methylene blue stain. **D-E** Tumor number and tumor load in each group were measured, *P < 0.05, **P < 0.01, t test. **F** Immunofluorescence staining of CD8 (red) and

DAPI (blue) in colon malignant tissues of WT C57BL/6 and IL-$6^{-/-}$ mice treated with AOM/DSS. Scale bar, 100 μm. **G** Immunofluorescent analysis of CD8 positive cells were assessed $^{**}P < 0.01$, *t* test. **H-J** Subcutaneous implantation of MC38 cells in C57BL/6 and IL-$6^{-/-}$ mice. 2×10^6 cells/mouse were injected into limbs; tumors were retrieved at 21th day after injection. (I) Tumor volume (cm^3) measured at indicated time point. $^{***}P < 0.001$, two-way ANOVA. (J) Tumor weight (H) measured at 21th day. $^{*}P < 0.01$, *t* test. (K) Positive numbers of $CD8^+$ staining, $^{**}P < 0.01$, *t* test. (L) Representative images of CD8 staining in subcutaneous tumor of each group. Scale bar, 100 μm.

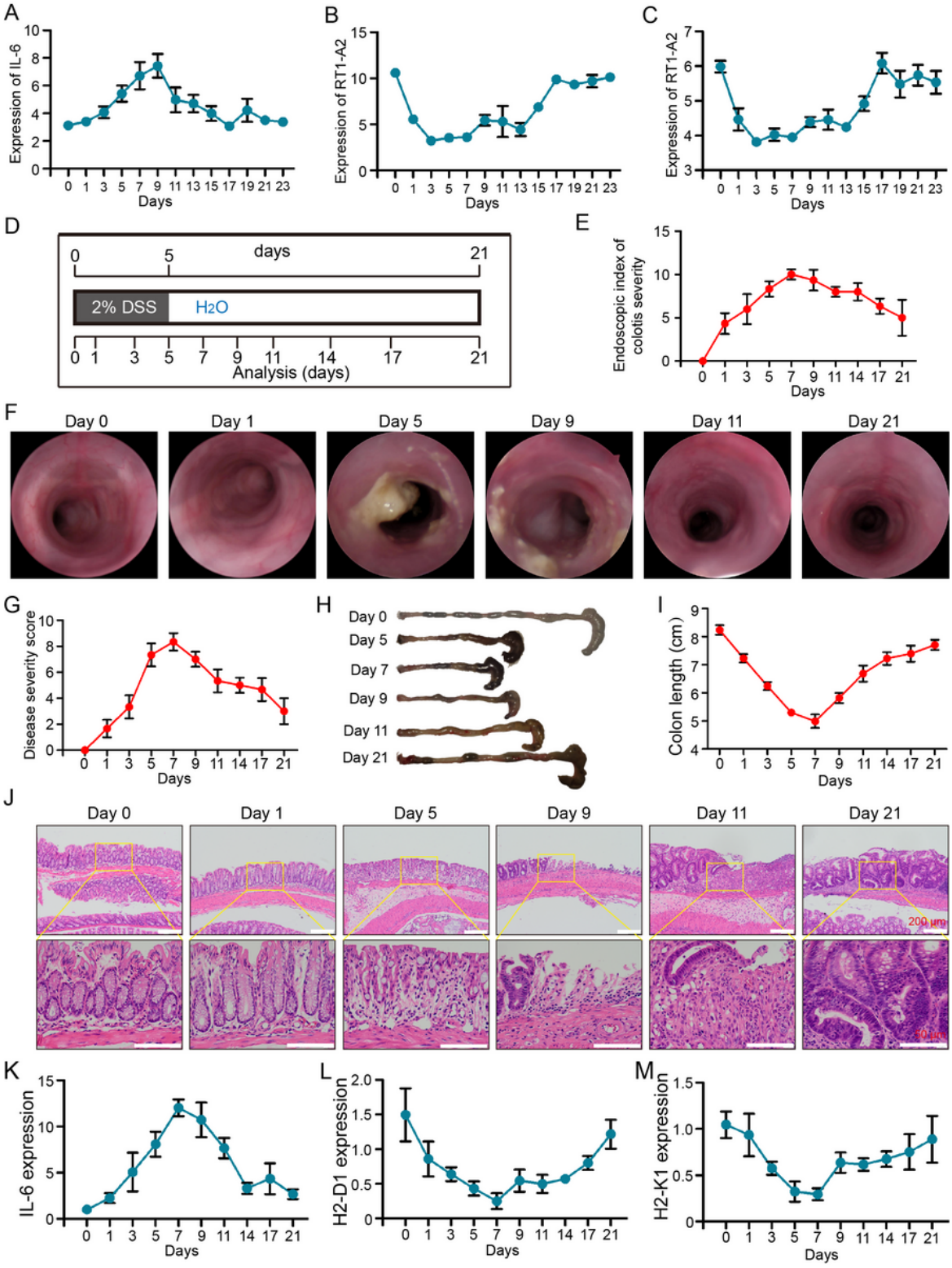

Figure 3

IL-6 produced in vivo was negative related to the expression of MHC-1 molecules

(A-C) The expression of IL-6, H2-D1 and H2-K1 in colonic mucosa of rats (n = 3) treated with DSS were analyzed using GEO data. **D** WT C57BL/6 mice (n = 6) were fed a 2% DSS solution in drinking water for 5 days. **E** Endoscopic index of colitis severity was scored until day 21 after the start of DSS. **F** Longitudinal

colonoscopic images of distal colon cross-sections of WT C57BL/6 mice (*n* = 6) at 0 and 1 day, and following 5, 9, 11 and 21 days of DSS treatment. **G** Disease severity was scored during DSS treatment. **H&I** Representative images and analysis of colon length at 0 and 1 day, and following 5, 9,11 and 21 days of DSS treatment(*n* = 6). **J** H&E staining of distal colon cross-sections of WT C57BL/6 mice (*n* = 6) at 0 and 1 day, and following 5, 9, 11 and 21 days of DSS treatment. Scale bar, 200 μm. **(K-M)** IL-6, H2-D1 and H2-K1 mRNA expression (qRT-PCR) of colonic mucosa from WT C57BL/6 mice (*n* = 3) fed with DSS.

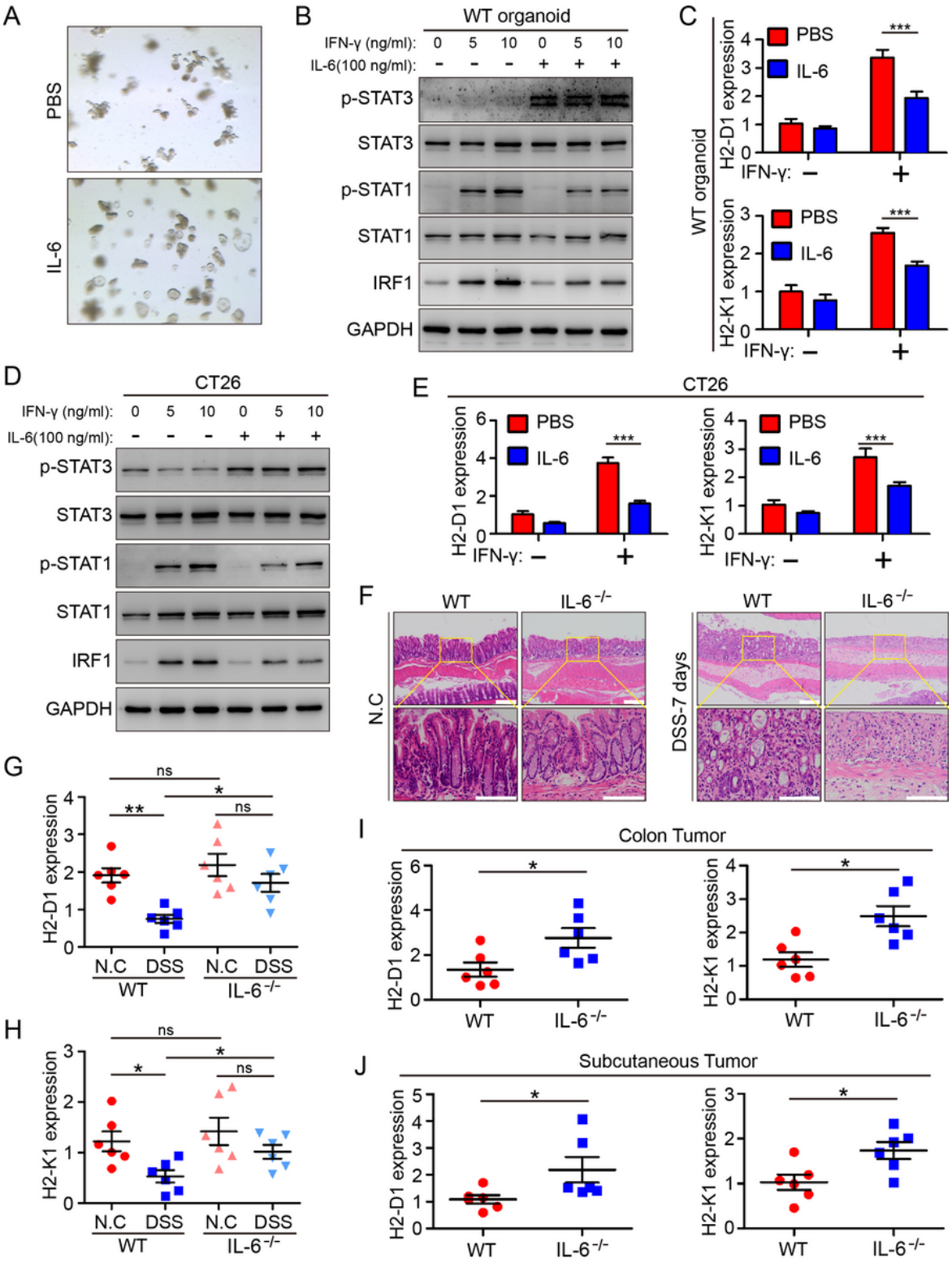

Figure 4

IL-6 deficiency induced the high expression of MHC-1 in vitro and in vivo

A Representative micrographs showing intestinal organoid derived from WT mice treated with PBS or IL-6. Scale bar, 200 μm. **B** Small intestinal organoids from WT C57BL/6 mice were stimulated with IFNγ and IL-6 with various concentrations, Expression of IRF1, STAT1, p-STAT1, STAT3 and p-STAT3 were examined by Western blotting. All samples were normalized as to expression of GAPDH. **C** qRT-PCR analysis of MHC-1 genes (H2-D1, H2-K1) in organoids from WT C57BL/6 mice (*n* =3) stimulated with IFNγ (50ng/ml) and IL-6 (100ng/ml) for 12-hours. ***$P < 0.001$, *t* test. **D** Colon carcinoma cell CT26 was stimulated with IFNγ and IL-6 in the same time with different concentrations, followed by extraction as total cell lysates, which subjected to immunoblot analysis with antibodies to the proteins stated above. **E** qRT-PCR analysis of MHC-1 genes (H2-D1, H2-K1) in CT26 cells stimulated with IFNγ (50ng/ml) and IL-6 (100ng/ml) for 12-hours. ***$P < 0.001$, *t* test. **F** H&E staining of colon sections from DSS-treated WT C57BL/6 and IL-$6^{-/-}$ mice at 0 and 7 days of DSS treatment. **G&H** qRT-PCR analysis of mRNA levels of the indicated MHC-1 target genes isolated from colon mucosa from WT C57BL/6 and IL-$6^{-/-}$ mice at 0 and 7 days of DSS treatment and normalized to GAPDH mRNA (*n* =6, per group). ns means no significance, *$P < 0.05$, **$P < 0.01$, one-way ANOVA. **I** qRT-PCR analysis of mRNA levels of the indicated MHC-1 target genes in tumors isolated from AOM/DSS models.*$P < 0.05$, *t* test. **J** qRT-PCR analysis of mRNA levels of the indicated MHC-1 target genes in subcutaneous tumors from the two groups. *$P < 0.05$, *t* test.

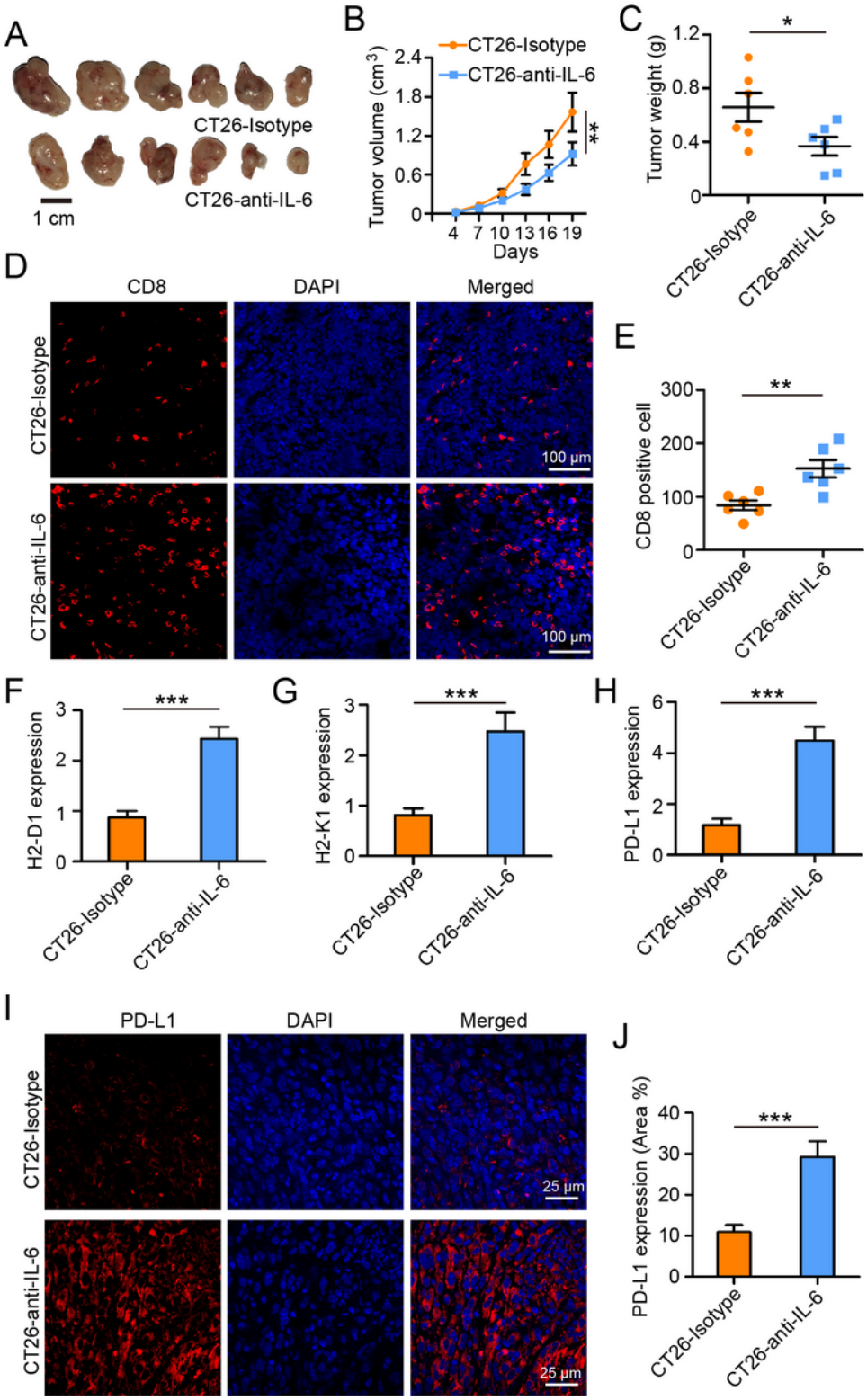

Figure 5

Anti-IL-6 enhanced infiltration of CD8$^+$ T cells in tumors via increasing the expression of MHC-1 and PDL-1

A Mice were implanted with CT26 cells and 19 days later retrieved. **B** Shown are tumor growth curves (*n* = 6 mice/group). Statistical significance determined using two-way ANOVA in comparison with control-

treated mice. **$P < 0.01$ **C** Evaluation of tumor weight is shown for each group. *$P < 0.05$, *t* test. **D-E** Immunofluorescence was used to analyze the staining of $CD8^+$ T cells infiltrating in CT26 tumor and quantification of positive $CD8^+$ T cells. Scale bar, 100 μm. **$P < 0.01$, *t* test. **F-H** MHC-1(H2-K1 and H2-D1) and PDL-1 mRNA levels were measured by q-PCR ***$P < 0.001$, *t* test. **I-J** Representative images of immunofluorescence microscopy to detect. (I) PDL-1protein expression (Red). Scale bar, 25 μm. (J) Percentage of PDL-1 were evaluated treated with anti-IL-6 or isotype. ***$P < 0.01$, *t* test.

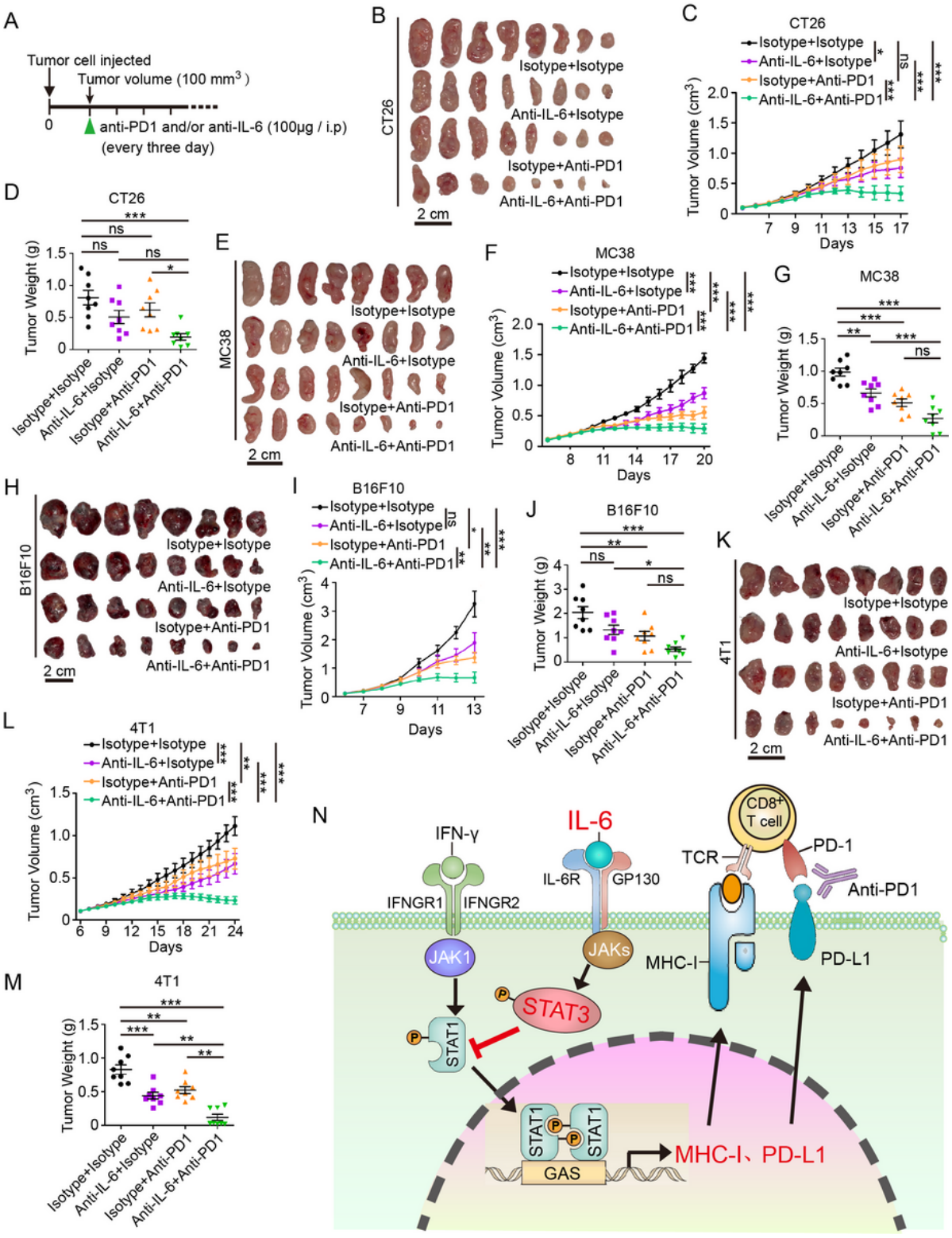

Figure 6

anti-IL-6 and anti-PD-1 combination therapy inhibits tumor growth in mice subcutaneous models

A Therapy regimen schematic. Tumor cells were injected into C57BL/6 or BAL b/c mice (*n* = 8 per group). Subsequently, when tumor volume reached about 100mm^3, 10 μg (100 μg/ml, 100μl) of anti-PD-1 and/or anti-IL-6 were injected into the mice every three days until sacrifice, while the control group was injected with isotype. **B-M** Anti-IL-6 was tested alone and in combination with anti-PD-1 in **(E & H**) C57/BL6J and (B & **K**) BALB/c implanted with (**E**) MC38, (**B**) CT26, (**H**) B16F10 or (**K**) 4T1 tumor cells. Tumor volume is represented as the mean ± SEM. (C, F, I, L) Individual tumor growth curves is presented for each treatment group compared with the control group. ns, no significance, **P* < 0.05; ***P* < 0.01; *** *P* < 0.001, two-way ANOVA. (D, G, J, M) Tumor weigh of subcutaneous tumors treated with PD-1/IL-6 monoclonal antibody respectively or anti-PD-1 with anti-IL-6. ns, no significance; **P* < 0.05; ***P* < 0.01; *** *P* < 0.001, *t* test. **N** Schematic diagram of the involvement of IL-6 in tumor evasion